Properties of amorphous carbon–silicon alloys deposited by a high plasma density source

B. Racine, A. C. Ferrari,[a] N. A. Morrison, I. Hutchings, W. I. Milne, and J. Robertson
Department of Engineering, Cambridge University, Cambridge CB2 1PZ, United Kingdom

(Received 13 April 2001; accepted for publication 1 August 2001)

The addition of silicon to hydrogenated amorphous carbon can have the advantageous effect of lowering the compressive stress, improving the thermal stability of its hydrogen, and maintaining a low friction coefficient up to high humidity. Most experiments to date have been on hydrogenated amorphous carbon–silicon alloys (a-$C_{1-x}Si_x$:H) deposited by rf plasma enhanced chemical vapor deposition. This method gives alloys with sizeable hydrogen content and only moderate hardness. Here we use a high plasma density source known as the electron cyclotron wave resonance source to prepare films with higher sp^3 content and lower hydrogen content. The composition and bonding in the alloys is determined by x-ray photoelectron spectroscopy, Rutherford backscattering, elastic recoil detection analysis, visible and ultraviolet (UV) Raman spectroscopy, infrared spectroscopy, and x-ray reflectivity. We find that it is possible to produce relatively hard, low stress, low friction, almost humidity insensitive a-$C_{1-x}Si_x$:H alloys with a good optical transparency and a band gap well over 2.5 eV. The friction behavior and friction mechanism of these alloys are studied and compared with that of a-C:H, ta-C:H, and ta-C. We show how UV Raman spectroscopy allows the direct detection of Si–C, Si–H_x, and C–H_x vibrations, not seen in visible Raman spectra. © *2001 American Institute of Physics.* [DOI: 10.1063/1.1406966]

I. INTRODUCTION

Amorphous carbon–silicon alloys (a-$C_{1-x}Si_x$) and hydrogenated carbon–silicon alloys (a-$C_{1-x}Si_x$:H_y) are of interest both in the Si-rich and C-rich composition range. The Si-rich alloys have a wider band gap than a-Si:H and are widely used as p-type window layers in a-Si:H based solar cells.[1–3] However, the addition of carbon worsens their photoelectronic properties, such as photoconductivity, because it increases the density of electronic defect states. This deterioration can be minimized by H dilution.[4] The C-rich alloys are also of interest as luminescent materials.[5,6]

The C-rich alloys are of interest as mechanical coating materials. A–C:H films with a significant fraction of C–C sp^3 bonding are referred to as diamond-like carbon (DLC).[7–9] This material is very useful as a hard protective coating due to its high hardness, low friction coefficient,[10] and good chemical stability, which derive directly from its sp^3 bonding. However, the use of DLC as a coating material is limited by three factors. First, it has a large compressive stress,[11] which limits the maximum thickness. Second, the low friction coefficient only occurs at low humidity;[12,13] it rises to 0.4–0.6 at a humidity of 50%. Third, thermal stability can be poor.[14] The addition of Si to a-C:H has the beneficial effect of reducing the grown-in compressive stress, improving the thermal stability, and maintaining the low friction coefficient of a-C:H to a higher relative humidity.[15–24]

The compressive stress of DLC arises from the deposition process itself, from the physical ion bombardment or subplantation used to create the metastable sp^3 bonding.[25,26,11] The stress is therefore intrinsic to DLC produced in this way. It was realized that addition of Si to a-C:H could promote sp^3 bonding by chemical means, rather than physical ion bombardment, and so it might not be accompanied by a compressive stress. Of course, Si–C bonds are not as strong as C–C bonds, so the benefits require that Si addition create enough C sp^3 sites.

The second problem is the thermal stability of H. Although sp^3 bonding is metastable, the H-free high sp^3 tetrahedral amorphous carbons (ta-C) can be stable in vacuum up to 1100 °C.[27,28] The thermal instability of a-C:H arises mainly from the instability of its bonded H.[14,29,30] The H starts to move around the network at about 350 °C and can evolve at 350–600 °C, depending on the quality of the a-C:H and on the vacuum conditions. The H evolution leads to a loss of sp^3 bonding, and its desirable mechanical properties. Si addition is found to raise the H evolution temperature up to 700 °C.[23]

The coefficient of friction of a-C:H can be very low, well below 0.1 in some cases.[12,31] However, for a-C:H this value is maintained only at low relative humidity (less than 1%), and it increases strongly to values of 0.2–0.6 at a typical humidity of 50%–80%.[12,13,32,33] It was found that Si addition would allow a-C:H to maintain the low friction coefficient to a typical humidity.[15]

On the other hand, the addition of C–Si bonds into a-C:H has the disadvantage of reducing the hardness and wear protection. The standard forms of a-C:H deposited by rf PECVD or reactive sputtering already actually contain a rather low fraction of C–C sp^3 bonding.[9] They therefore have an elastic modulus and a hardness only 10%–20% of that of a fully sp^3 bonded network or of diamond itself. PECVD a-C:H has a maximum hardness of about 20 GPa and a maximum Young's modulus of about 200 GPa.[34] This hardness is somewhat too low to confer wear protection

[a]Electronic mail: acf26@eng.cam.ac.uk

 © 2001 American Institute of Physics

Downloaded 04 Dec 2006 to 129.169.177.41. Redistribution subject to AIP license or copyright, see http://jap.aip.org/jap/copyright.jsp

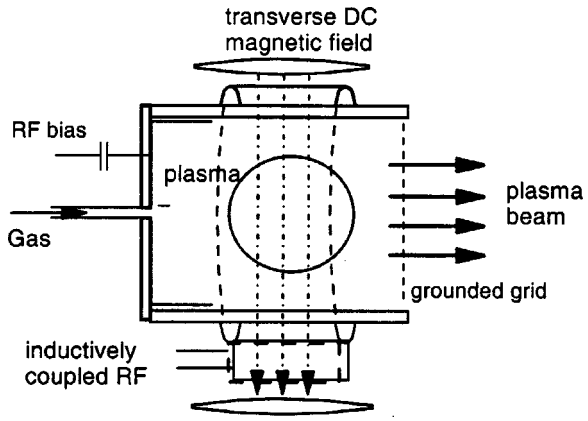

FIG. 1. Schematic diagram of the ECWR source.

against oxides used in magnetic tapes such as Cr_2O_3, for which hardness over 30 GPa is needed.

The low fraction of C–C bonding arises because in a capacitively coupled rf PECVD reactor, only about 10% of the film-forming species are energetic ions, which directly promote the sp^3 bonding.[35] The rest are neutral species with no energy, and these do not promote sp^3 bonding. It is necessary to use high plasma density reactors to deposit *a*-C or *a*-C:H films with a much higher ionized fraction of incident species.[36] Examples of high plasma density reactors are cathodic arcs, inductively coupled sources, electron cyclotron resonance sources, the plasma beam source,[36] and the electron cyclotron wave resonance (ECWR) source as used here.[37,38] Such sources give rise to *a*-C or *a*-C:H with a much higher C–C sp^3 bonding fraction, which are called *ta*-C or *ta*-C:H, respectively.[26,35] These films have much larger densities, elastic moduli, and hardnesses.[36,39,40] This article describes the preparation and the structural, optical, and tribological properties of the Si alloys of *ta*-C:H.

II. EXPERIMENT

A. Deposition

The ECWR[37,38] is a 13.6 MHz single turn, inductively coupled source, see Fig. 1. A transverse magnetic field is generated via the Helmholtz coils and it splits the electromagnetic waves into two circularly polarized waves. The right-hand polarized wave is no longer reflected by the plasma, but is strongly coupled to the bulk plasma. This allows an efficient power transfer from the rf into the plasma, and enables the formation of a plasma density two orders of magnitude or more greater than in a capacitive source. A resonant condition is achieved when a standing wave is set up within the source cross section.[38] A plasma beam exits through a grounded tungsten grid. A rf-excited bias electrode opposite the grid acquires a dc self-bias potential and is used to control the ion energy of the plasma beam.

The films are deposited from a mixture of acetylene and silane onto silicon or quartz substrates at room temperature. The gas flow ratio $R=[SiH_4(\text{sccm})]/([C_2H_2(\text{sccm})]+[SiH_4(\text{sccm})])$ is varied from 0 to 1 to produce *a*-$C_{1-x}Si_x:H_y$ alloys ranging from *ta*-C:H to *a*-Si:H. All the other deposition conditions were kept fixed. The operating pressure of $\sim 1.2\times 10^{-3}$ mbar was maintained by a turbomolecular pump with a pumping speed of 1600 l/s. The rf power was 285 W, and the voltage and current across the Helmholtz coils were 4.7 V and 980 mA, respectively, which gave an ion energy of ~150 eV for a pure C_2H_2 plasma.[38] The ion energy distribution of the pure C_2H_2 plasma was measured by Faraday cup and is relatively sharp at this low pressure because there are few collisions in the plasma sheath.[38] The films were deposited at room temperature because this work focuses on C-rich alloys with primarily mechanical applications, and higher deposition temperatures can lead to more C sp^2 bonding. On the other hand, the electronic properties of the Si-rich alloys would be improved by using a higher deposition temperature.

B. Characterization

The deposited films were characterized in terms of their structural, mechanical, and optical properties. The film thickness and refractive index were determined by ellipsometry at 633 nm. The films are about 35–65 nm thick. The film stress was determined using Stoney's equation. The surface curvature of the Si substrate, before and after deposition, was measured by profilometry. The optical gap (E_{04} and Tauc) and the complex refractive index were measured with a UV-visible spectrophotometer.

The chemical bonding within the films was determined by using Fourier transform infrared spectrometry (FTIR). The C/Si ratio in the films and the H content were determined by a combination of x-ray photoelectron spectroscopy (XPS), Rutherford backscattering (RBS), and elastic recoil detection analysis (ERDA). The density of the films was determined by x-ray reflectivity (XRR). The XRR curves were measured on a Bede Scientific GIXR reflectometer, with a Bede EDRA scintillator detector using monochromatized Cu $K\beta(\lambda=1.3926\,\text{Å})$ radiation. The structure of the films was also studied by a combination of visible and UV Raman spectroscopy. Visible Raman spectra at 514.5 nm were collected on a Renishaw micro-Raman 2000 spectrometer. UV-Raman spectra at 244 nm were collected on a UV-enhanced charge coupled device (CCD) camera on a Renishaw micro-Raman system 1000, modified for use at 244 nm with fused silica optics. The sp^3 fraction was derived by electron energy loss spectra (EELS). EELS measurements were carried out on a dedicated VG501 scanning transmission electron microscope fitted with a spectrometer with a McMullan parallel EELS detection system.[40]

Friction measurements were performed for 2 h on a ball-on-disk tribometer. Stainless steel balls (AISI 52100, 6.35 mm diameter) were used during the tests, which were conducted both in air and under a controlled humidity environment (from 10% to 80% relative humidity). A load of 2N was applied, corresponding to a Hertzian contact pressure of 370 MPa. A sliding speed of 0.5 cm/s was used in each measurement. A second series of friction measurements were performed with DLC-coated steel balls. For this an *a*-C:H layer was deposited by a PECVD system at 200 W and 100 mTorr pressure. In these conditions a typical diamond-like *a*-C:H is obtained on Si with a Tauc gap of ~1.5 eV.

Downloaded 04 Dec 2006 to 129.169.177.41. Redistribution subject to AIP license or copyright, see http://jap.aip.org/jap/copyright.jsp

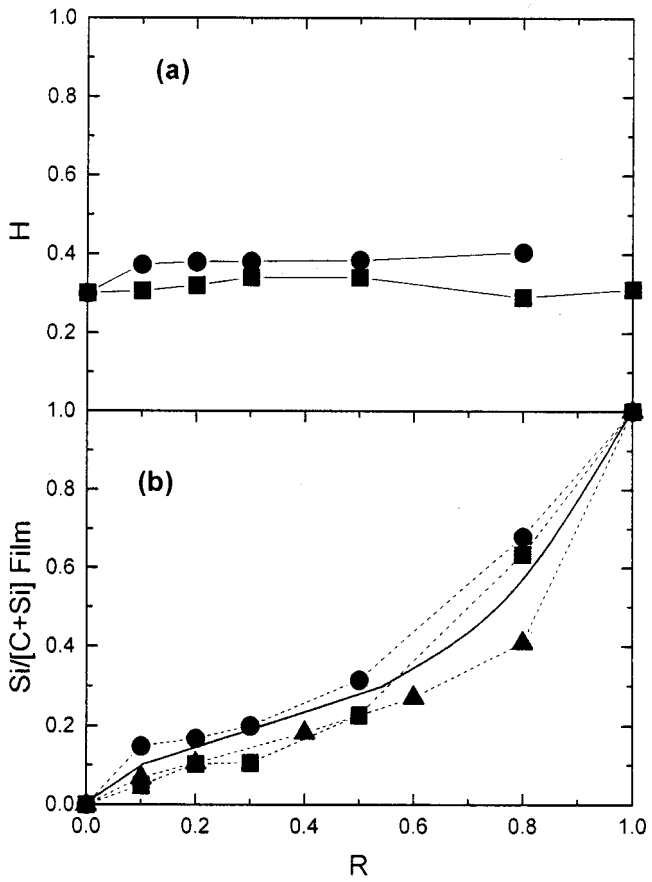

FIG. 2. (a) Hydrogen content and (b) Si/(C+Si) ratio as a function of the gas flow ratio *R*. (■) and (●) derive from RBS+ERDA measurements on two different series of samples grown in similar conditions; data-points (▲) derive from XPS measurements on the same samples as (■). The solid line in (b) is the best estimate of the composition vs *R*.

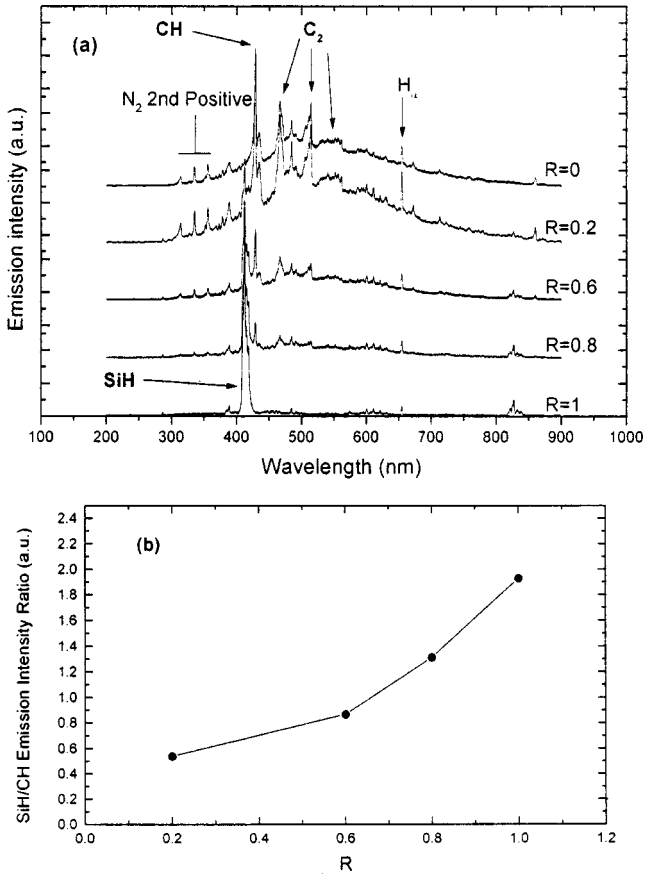

FIG. 3. (a) Optical emission spectra of SiH_4/C_2H_2 plasma for different *R* values. (b) Variation of SiH to CH intensity ratio with *R*.

III. RESULTS AND DISCUSSION

A. Film composition

Figure 2 shows the variation of the silicon atomic fraction, Si/(Si+C), and hydrogen content in $a\text{-}C_{1-x}Si_x:H_y$ alloys as a function of the gas flow ratio *R*. It can be seen that the Si content increases slowly until $R\sim0.6$ and it then increases strongly thereafter. The stoichiometric composition $x=0.5$ corresponds to a flow ratio of $R\sim0.75$. This is consistent with the optical gap data discussed in Sec. III F.

This is an unexpected result in that C seems to be more readily incorporated than Si in the deposited film. The incorporation efficiency of C is low in $a\text{-}C_{1-x}Si_x:H_y$ alloys produced by conventional rf-PECVD from methane/silane mixtures[41–46] because methane possesses both a higher ionization energy and higher dissociation energy than silane. An extreme form of this behavior is seen at low rf powers by Solomon *et al.*[46] In contrast, high plasma density reactors with a high electron temperature and plasma density allow a high dissociation of both precursors, and this usually gives a relatively linear dependence of film composition on gas flow ratio. Typical examples of this behavior are found in the ECR deposition of $a\text{-}C_{1-x}Si_x:H_y$ alloys found previously by Conde *et al.*[47] and Yoon *et al.*[48]

To understand our result further, the plasma was analyzed by optical emission spectroscopy (OES). Figure 3(a) compares the emission spectra for various *R* values. The spectra show a high degree of dissociation in the plasma, through the appearance of the SiH, CH, C_2, and H_α bands at ~410.9, 428.6, 513.3, and 656.2 nm, respectively.[49] Assuming that species concentrations are monotonically related to emission intensities, the data in Fig. 3(b) indicate that the active Si/C ratio in the plasma rises substantially for flow ratios *R* above 0.6. This is also where the incorporation efficiency of Si increases strongly. As the activation energies for dissociation and ionization of silane are lower than those of acetylene,[50] it is likely that the deactivation of silicon containing precursors in the gas-phase occurs by dimerization (e.g., $SiH_3+SiH_3\rightarrow Si_2H_6$). As the residence time and mean free path are both very low in our reactor (~0.8 ms and ~10 cm), these reactions provide a thermodynamically accessible route[51] to fewer active silicon species in the plasma. Furthermore, thermodynamics indicate that the formation of C–C bonds are favored over the formation of either Si–C or Si–Si bonds at the surface. Hence significant levels of Si incorporation are only possible when the active silicon content in the plasma is significantly greater than that of the active carbon precursor species.

The hydrogen content in the films remains almost constant at 30%–40% and is independent of *x*, Fig. 2(a). This is similar to the results of Camargo *et al.*[23] It contrasts with the

Downloaded 04 Dec 2006 to 129.169.177.41. Redistribution subject to AIP license or copyright, see http://jap.aip.org/jap/copyright.jsp

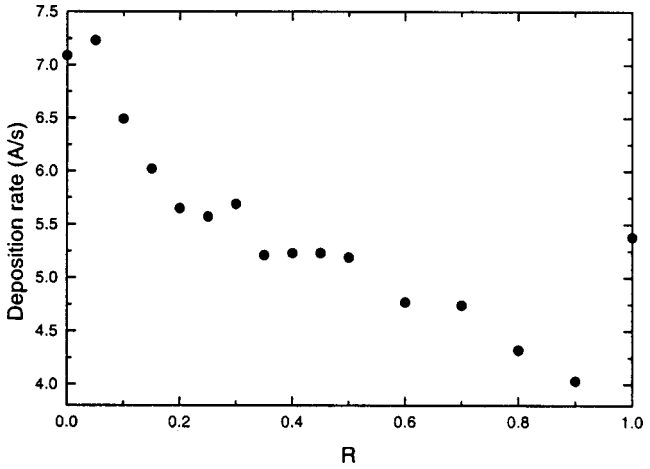

FIG. 4. Deposition rate vs *R*.

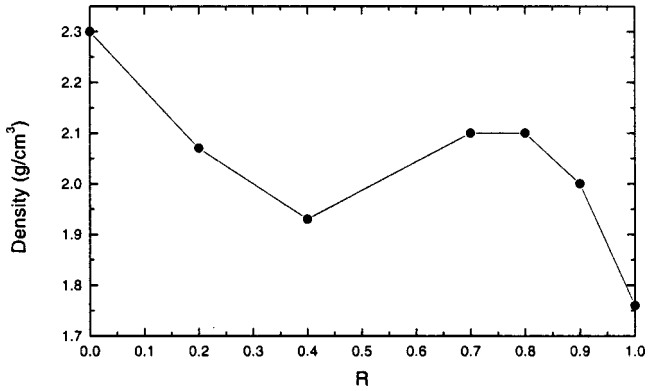

FIG. 5. Variation of density determined by x-ray reflectivity as a function of *R* for samples (■) of Fig. 2.

variation found for films deposited by conventional PECVD, where the H content increases strongly in C-rich films.[52] The high H content in PECVD films is due to the incorporation of C as CH_3 groups,[46] while Si is incorporated as SiH or SiH_2 groups. The CH_3 radical is the dominant hydrocarbon radical in rf-PECVD methane plasmas.[53] We used acetylene (C_2H_2), which gives films with less H because the carbon is not incorporated mainly as–CH_3.[43,54] As the electron temperatures and plasma densities are so high in ECWR plasmas, significant concentrations of atomic H have previously been found when using either hydrocarbon or silane precursors. Hence reasonable levels of H incorporation can be expected, irrespective of the gas flow ratio used, if a super-equilibrium of atomic hydrogen exists in the gas phase. The high H content of our Si-rich alloys is because the deposition is carried out at room temperature, in contrast to most others.

B. Growth rate

Figure 4 shows the variation of the deposition rate with gas flow ratio *R*. The rate decreases slightly from 7.5 to 4.5 Å/s with increasing *R*. Our result is similar to the deposition rate reported by Oguri *et al.*[15,16] and Gangopadhyay *et al.*,[22] but it is 5–10 times higher than for the ECR deposited films of Conde *et al.*[47]

The trend of our deposition rate is opposite to that of Conde *et al.*[47] and Jiang *et al.*[43] for PECVD films, where the deposition rate increases with *R*. The decrease in deposition rate with increasing *R* in our work could arise from a number of factors. It may reflect the lower incorporation efficiency of Si compared to C in our films. Alternatively it may be due to more etching/sputtering reactions because of the lower strength of Si–C than C–C bonds.[50]

C. X-ray reflectivity

Grazing incidence x-ray reflectivity (XRR) is an efficient, nondestructive, parameter-free means to measure the mass density of thin films.[40] The refractive index of x rays in solids is slightly less than unity, so external reflection occurs at low angles of incidence. As the grazing incidence angle increases above a critical angle θ_c, x-rays start to penetrate in the film. XRR measures the intensity reflected in the specular direction as a function of the grazing incidence angle.

The critical angle, θ_c, of total external reflection of x rays from a material with elements j of molar masses M_j and density ρ_j is given by

$$\theta_c = \lambda \left(\frac{N_A r_0}{\pi} \sum_j \frac{\rho_j}{M_j} (Z_j + f_j') \right)^{1/2}, \tag{1}$$

where λ is the x-ray wavelength (1.3926 Å in our experiment), $r_0 = e^2/4\pi\varepsilon_0 m_e c^2$ is the electron classical radius, m_e is the electron mass, N_A is the Avogadro number, and f_j includes dispersive and absorptive corrections.[40] We previously gave a formula to derive the density from the critical angle for films composed of carbon, hydrogen, and nitrogen.[40] For a-$C_{1-x}Si_x$:H_y alloys we must consider carbon, hydrogen, and silicon:

$$\theta_c = \lambda \left(\frac{N_A r_0}{\pi} \times \rho \frac{[X_C(Z_C + f_C') + X_H(Z_H + f_H') + X_{Si}(Z_{Si} + f_{Si}')]}{(X_C M_C + X_H M_H + X_{Si} M_{Si})} \right)^{1/2}, \tag{2}$$

where ρ is the overall mass density. We have $f_C' \approx 10^{-2}$, $f_H' \approx 10^{-4}$, and $f_{Si}' \approx 0.28$ (in electron units).[55] Thus we neglect dispersion corrections except for Si. As $X_H = 1 - X_C - X_{Si}$, we have

$$\rho \cong \frac{\pi^2 c^2 \varepsilon_0}{3\lambda^2 N_A e^2} M_C m_e \theta_c^2 \frac{11X_C + 27.1X_{Si} + 1}{5X_C + 13.3X_{Si} + 1}, \tag{3}$$

where e is the electron charge and ε_0 is the dielectric permittivity of vacuum.

Figure 5 plots density (± 0.1 g/cm^3) vs *R*. We see that after an initial decrease of ~10%, the density remains at ~2.1 g/cm^3 up to $R = 0.8$, $x = 0.6$. This would suggest that the mechanical properties do not significantly decline with respect to the as -deposited ta-C:H. Note that the density of our a-Si:H is small due to the high H content.

XRR gives also the layering, thickness, and roughness of the films. The roughness is about 5–7 Å. A lower density surface layer of ~1–2 nm is found up to $R = 0.7$, but this

Downloaded 04 Dec 2006 to 129.169.177.41. Redistribution subject to AIP license or copyright, see http://jap.aip.org/jap/copyright.jsp

layer becomes thinner at higher R, and is not detectable for $R=1$. This is an interesting result. An outer layer is commonly found in amorphous carbons.[26,40] This arises directly from the deposition mechanism known as subplatation, in which the films grow from energetic ions by subsurface growth, thereby creating a less dense outer layer. The fact that the outer layer declines for increasing R confirms that Si is tending to promote sp^3 bonding in a-C:H by chemical means, rather by the physical subplantation mechanism. This physical ion bombardment is the main cause of stress build up in amorphous carbons. We thus expect a lower stress with higher Si content and this is observed in Sec. III G.

D. Infrared absorption

FTIR gives valuable information on the local bonding. The spectra of a-$C_{1-x}Si_x$:H_y alloys broadly consist of three regions:[1,44,47,56–60] the C–H bond stretching modes around 3000 cm^{-1}, the Si–H stretching modes around 2000 cm^{-1}, and the Si–C stretching and Si–H_n bending modes below 1600 cm^{-1}. Figure 6(a) plots the spectra in the low wavenumber region. The features here are Si–C, C–C, and Si–Si stretching modes, together with bending modes of C–H and Si–H groups. The spectra consist of a main broad band at 770 cm^{-1} with a shoulder at ~980–1000 cm^{-1}, slightly upshifting with decreasing R. The intensity of the 770 cm^{-1} band has a maximum at $R=0.8$ or $x\sim0.5$–0.6. This band is completely lost at $x=1$, where there is the ~650 cm^{-1} band, due to the SiH_n bending modes,[56] and the characteristic bending doublet at 845–890 cm^{-1}.[56,57] The mode assignment in this region has been controversial. Based on Si-alkane molecules, Wieder *et al.*[57] assigned the 670 cm^{-1} mode to Si–C bond stretching and the 780 cm^{-1} mode to Si–CH_3 wagging. However, the Si–C stretching mode occurs at ~ 780 cm^{-1} in sputtered a-SiC and in annealed SiC,[1] so the assignments are not clear-cut and it is possible that the two bands could intermix.[44] For our spectra, it is important to note that the high dissociation means that CH_3 groups are unlikely to be present in high amounts. Our spectra are notably broad and bandlike, rather than sharp and molecular-like as in Tawada *et al.*[2] Thus the 770 cm^{-1} band can be assigned here to Si–C. The band at ~ 980–1000 cm^{-1} is usually assigned to wagging vibrations of CH_n bonds in Si–CH_n groups.[1,44,47,57,59]

Figure 6(b) shows the high frequency part of the infrared spectra, with the Si–H stretching modes around 2000 cm^{-1} and the C–H_x modes around 3000 cm^{-1}. A detailed analysis of the 2800–3100 cm^{-1} band shows that it changes with R. For $R=0$, in ta-C:H, the band peaks at ~ 2900 cm^{-1}, corresponding to sp^3 C–H stretching modes and at ~3065 cm^{-1} due to sp^2 C–H bond stretching.[54] The latter band disappears for $R>0.2$ or $x=0.07$. At the same time, the lower frequency band gains intensity at ~2870 cm^{-1} due to sp^3 $CH_{2,3}$ symmetrical stretching modes[54] and becomes the main C–H stretching band left for $R=80\%$, $x=0.5$–0.6. Since the total amount of H is roughly constant and the intensity of this band for $R=0.8$ is very small, we assume that a significant fraction of C is bonded only to Si atoms. This confirms that $R=0.8$ films are quite chemically ordered, and have the highest Si–C bonding and high sp^3 content, consistent with the high optical gap, as discussed in Sec. III F. A similar trend in the Si–C and Si–H vibrations is seen in the UV Raman data discussed in Sec. III E.

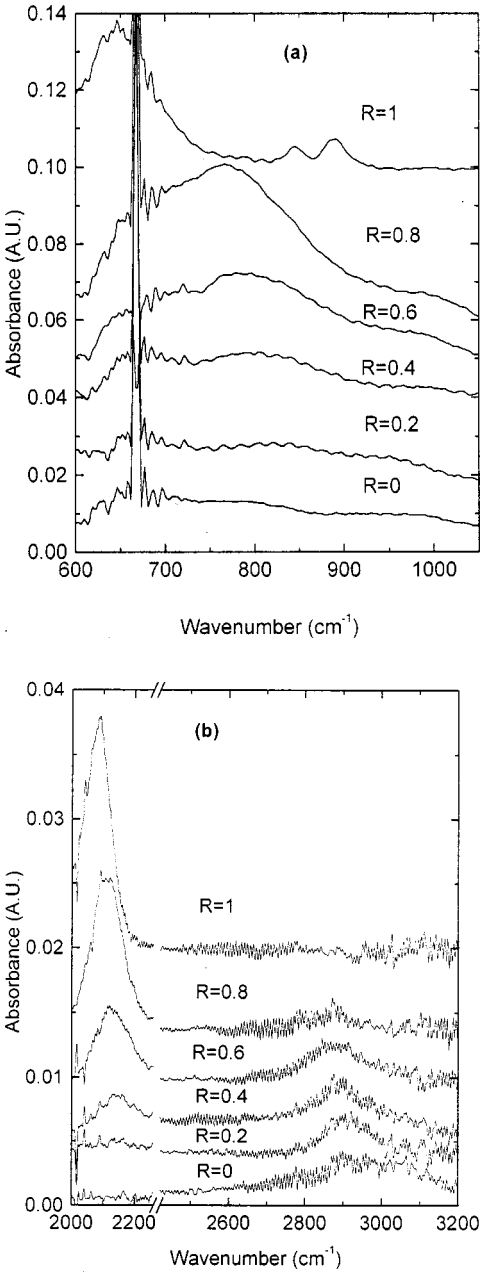

FIG. 6. (a) Low frequency FTIR spectra of a series of samples with increasing R. (b) High frequency FTIR spectra of the same samples. Note that our FTIR spectra were measured in air. The sharp peak at ~670 cm^{-1} is due to atmospheric CO_2; no useful information could be obtained in the 1200–2000 cm^{-1} region due to the prominent water vapor contribution.

The intensity of the Si–H modes is seen to increase with increasing x, as expected. In our a-Si:H, the SiH band is dominated by the modes of the SiH_2 group at ~2090 cm^{-1}, with a very small contribution at ~2000 cm^{-1} due to the SiH group.[56] We thus fitted this band with a single Lorentzian. The position of this peak shifts to higher wave numbers with increasing C content (Fig. 7). This shift is due to the induction effect of substituting neighbors of higher electronegativity into the a-Si:H network.[60] Carbon has a higher electrone-

Downloaded 04 Dec 2006 to 129.169.177.41. Redistribution subject to AIP license or copyright, see http://jap.aip.org/jap/copyright.jsp

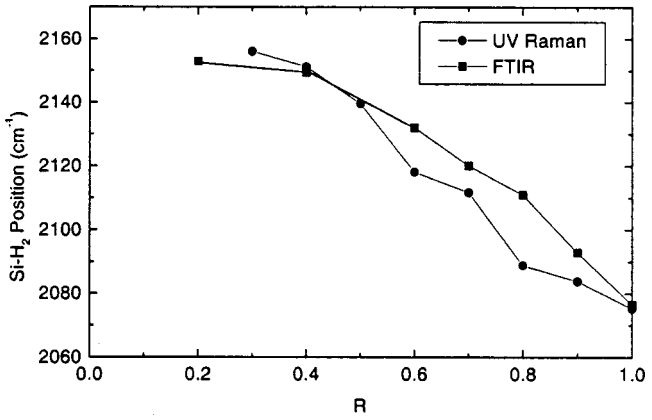

FIG. 7. Variation with R of the $Si–H_2$ stretching mode position, as detected in FTIR and UV Raman spectroscopy. For simplicity the peak was fitted with a single Lorentzian, neglecting the lower frequency Si–H contribution, which is also present.

gativity than Si, and so attracts electrons from it, which shortens the Si–H bond and increases its vibrational frequency.[60]

It should be noted that the thermal stability of *ta*-C:H is already much better than that of *a*-C:H, with hydrogen evolution occurring at 700 °C,[54,61] rather than 400–600 °C.[14] This is due to the denser network of *ta*-C:H. Thus Si addition is not likely to further improve the stability, unlike in *a*-C:H itself.[23]

E. Raman spectroscopy

The Raman spectra provide valuable information on the alloy structure. The visible Raman spectra for various compositions are shown in Fig. 8(a). The spectra of C-rich alloys are dominated by the *G* peak of the C–C network at around 1530 cm^{-1} with a weaker shoulder known as the *D* peak at 1350 cm^{-1}. The *G* peak is due to the bond stretching of sp^2 carbon atom pairs, while the *D* peak is due to breathing modes of aromatic clusters.[62] The sharp first and second order Si peaks are due to the Si substrate, while in Si-rich alloys the Si–Si peak at 490 cm^{-1} of the *a*-Si network is superimposed to the substrate signal.

The 514 nm Raman spectra of the C-rich alloys are dominated by the C sp^2 sites, which have a 50–230 times higher Raman scattering efficiency than the sp^2 sites.[62] They give information mainly on the configuration of the sp^2 sites and the size of the sp^2 clusters.[62] This is only indirectly related to other factors such as the sp^3 content. In *a*-C:H, the *G* peak downshifts with increasing gap and sp^3 content, from 1580 to about 1520 cm^{-1} for excitation at 514 nm. In *a*-C:H this is due to its increasingly polymeric nature, since the higher sp^3 content is achieved by a higher H content.[62] In $a\text{-}C_{1-x}Si_x:H_y$, the *G* peak shifts down more strongly, reaching 1410 cm^{-1} for $R=0.8$, $x=0.5$–0.6. This almost linear shift with increasing Si content is a typical signature of $a\text{-}C_{1-x}Si_x:H_y$. This was first seen by Gorman and Solin[63] and Ramsteiner *et al.*[64] and then by many others.[41,59,65] This downshift is attributed to the lowering of C═C vibration modes by the heavier Si atoms in the C network. This effect must dominate the effect of any further localization of the

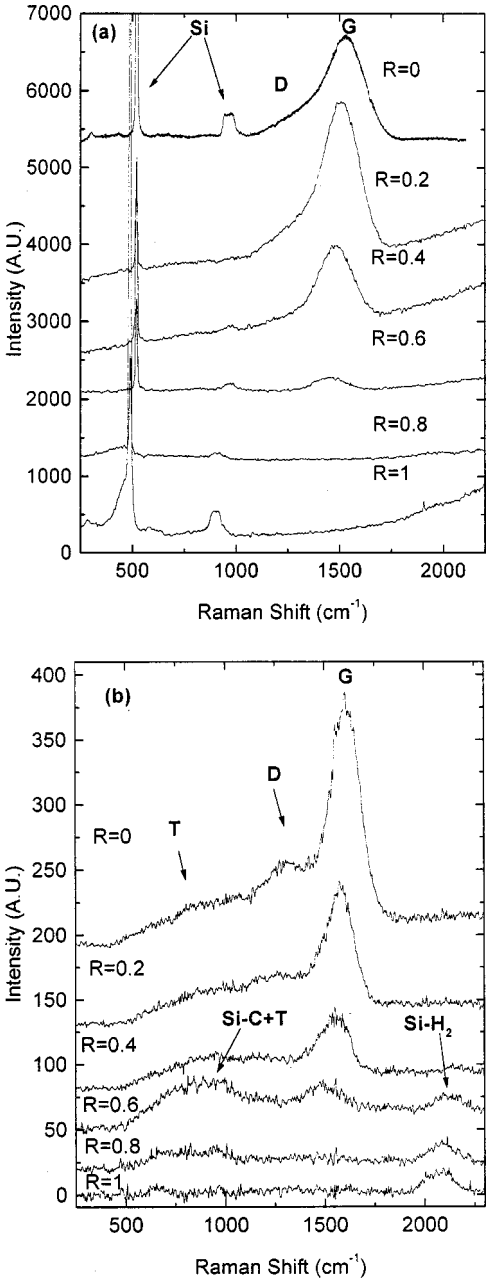

FIG. 8. (a) Visible Raman spectra of $a\text{-}C_x:Si_{1-x}:H_y$ alloys vs R for 514 nm excitation. (b) UV Raman spectra for 244 nm excitation. The major peaks are labeled.

sp^2 phase due to Si, which would tend to raise the *G* peak.[62] An additional cause of downshifting could be the electron excess on the more electronegative C atoms linked to Si, resulting in weaker C═C bonds with lower vibrational frequencies.

To derive further information from the spectra, we analyzed them by fitting a Breit–Wigner–Fano (BWF) for the *G* peak, and Lorentzian for the *D* peak. The Lorentzian is a symmetric line shape, but the BWF can be skewed. We take the peak position of the BWF at its maximum rather than at its center.[62]

Figure 9 shows the variation of the *G* peak and the ratio of intensities of the *D* peak and *G* peak, $I(D)/I(G)$, for 514 nm excitation, and the *G* peak position for UV Raman exci-

Downloaded 04 Dec 2006 to 129.169.177.41. Redistribution subject to AIP license or copyright, see http://jap.aip.org/jap/copyright.jsp

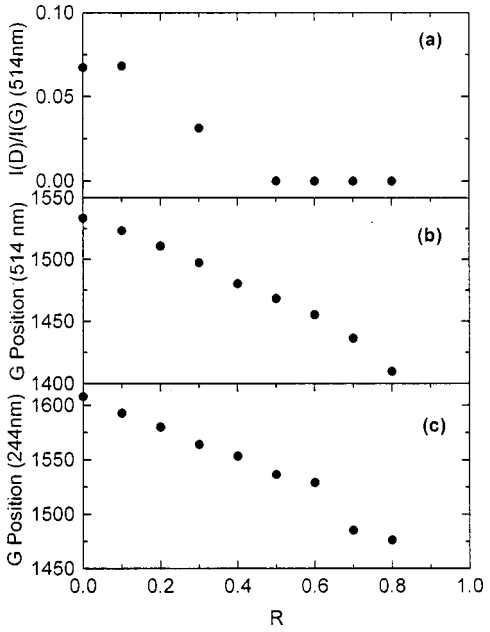

FIG. 9. Variation of (a) $I(D)/I(G)$ and (b) G position in 514 nm Raman spectra and (c) G position in UV Raman spectra vs R.

tation. The as-deposited ta-C:H films still show a small D peak, but this decreases rapidly with increasing x, falling to zero at $R=0.5$. This is reflected in the decrease of the ratio $I(D)/I(G)$. This occurs because increasing Si content opens up the remaining rings of C sp^2 sites, creating a olefinic sp^2 structure with a higher optical gap.[62]

The UV Raman spectra of DLCs are important because UV photons directly excite the sp^3 sites.[66,67] Figure 8(b) shows the UV Raman spectra of our films. The UV spectra are significantly different than those for visible excitation. The spectrum of ta-C:H has three main contributions: The G peak, the D peak, and a T peak at $\sim$980 cm^{-1}. The T peak, seen only for UV excitation, is due to the resonant enhancement of the σ states and directly probes the C–C sp^3 bonding. The intensity ratio of the T and G peaks can be used to estimate the sp^3 fraction.[68] For $R=0$, $I(T)/I(G)=0.14$, which indicates an sp^3 content of $\sim$70%,[68] as is confirmed by direct EELS measurements.

The shift of the G peak in UV Raman is very important. If it rises above 1600 cm^{-1}, it indicates that the sp^2 sites are predominantly in short chains and not in rings.[68] However, in a-$C_{1-x}Si_x$:H_y alloys damping effects of Si atoms dominate. The decrease of the $I(D)/I(G)$ ratio in visible and UV Raman means that Si reduces aromatic clusters, and this would tend to raise the G peak in Si-free films,[62] in contrast to the observed lowering in the a-$C_{1-x}Si_x$:H_y alloys.

Figures 9(b) and 9(c) show that the downshift of the G peak with increasing R in UV Raman spectra parallels the shift in visible Raman spectra, the G peak being $\sim$70 cm^{-1}higher in UV Raman spectra than in the 514.5 nm Raman spectra. This suggests that the C sp^2 sites have a unique configuration at a given Si content, as a different distribution of C sp^2 clusters would give a different trend in the UV and visible Raman spectra.[68] Indeed, neglecting the effect of Si mass, Raman ΔG(UV-visible) would increase with R for less sp^2 clustering.[68] This may allow the Si/C ratio to be directly derived from the Raman parameters, combining Figs. 2 and 9.[41] Hence we can assert that the C–C sp^2 content does not increase with Si addition. This is confirmed by EELS measurements that give an almost constant sp^3 fraction of $\sim$70% up to $R=0.4$.

A new result from our UV Raman measurements is that all the σ bonds become visible and we can now clearly detect Si–C, Si–H, and C–H bonds. Indeed, the band at 2100 cm^{-1} can be identified with the Si–H_2 stretching modes seen in FTIR. For simplicity we fitted this band in FTIR spectra and UV Raman spectra with a single Lorentzian. Figure 7 plots the position of this peak vs R, as derived by UV Raman and FTIR spectra. The good agreement of peak positions and redshift with increasing R between FTIR and UV Raman data confirms our assignment of this band in UV Raman spectra to Si–H_2 stretching modes.

The broad feature at 500–1000 cm^{-1} in UV Raman spectra is difficult to analyze at high R as it contains contributions from C–C sp^3 bonds, SiH_n bending modes, and Si–C modes. However, as the band's intensity does not decrease with respect to the G peak, this also indicates that the overall sp^3 content of our films does not fall at large R. Figure 10(a) compares the FTIR spectrum and the UV Raman spectrum of the a-Si:H film. The correspondence of the $\sim$650 cm^{-1} peak allows us to identify it as SiH_n bending in UV Raman spectra. Figure 10(b) compares the FTIR spectrum and the UV Raman spectrum of the sample with $R=0.8$, $x=0.5$–0.6. Apart from the 650 cm^{-1} peak, the UV Raman spectrum shows two extra peaks at $\sim$760 and $\sim$950 cm^{-1}. These two peaks can be identified as peaks in the phonon density of states of SiC,[69] which should be seen in a-SiC. Extremely weak peaks are sometimes seen in this region for visible Raman in a-SiC,[70–72] but usually nothing is seen.[73,44] This is due to the small cross section of Si–C in visible excitation. Note that the correspondence between the UV Raman and IR spectrum for Si–C vibrations is lost in this case, due to the different Raman and IR cross sections of the modes contributing to this spectral region. This is also reflected in the inversion of the intensities in the 500–1000 and 2100 cm^{-1} regions, with the Si–H_2 stretching modes more intense in the UV Raman spectra than the IR ones. Further studies are needed to define how to properly deconvolute the contributions in the 500–1000 cm^{-1} region of the UV Raman spectra for all the different C/Si compositions.

UV Raman spectra also detect C–H stretching modes.[68] Figures 11(a) and 11(b) compare the FTIR and UV Raman spectra in the 2900 cm^{-1} region for films at $R=0$, 0.4, and 0.8. The spectra shapes and the peak trends are similar. In addition UV Raman spectra show the $2G$ peak at least for low R. Figure 11 confirms the analysis of Sec. III D, that the main contribution for low R is the sp^3C–H stretching mode, and the $sp^3CH_{2,3}$ stretching mode at lower frequency becomes dominant at higher R.

F. Optical absorption

Figure 12 shows the variation of the refractive index n with gas flow ratio. The refractive index remains at 2.2 until

Downloaded 04 Dec 2006 to 129.169.177.41. Redistribution subject to AIP license or copyright, see http://jap.aip.org/jap/copyright.jsp

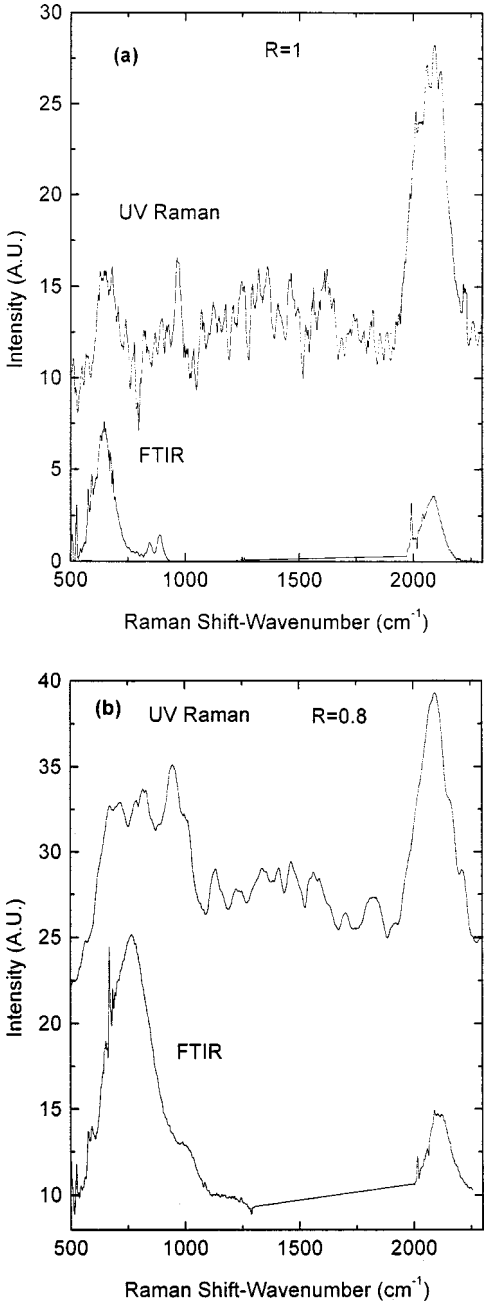

FIG. 10. Comparison of UV Raman and FTIR spectra for (a) a-Si:H ($R=1$) and (b) a-C_{1-x}:Si_x:H_y grown at $R=0.8$, $x=0.5$–0.6. The UV Raman spectra have been smoothed for clarity. In the FTIR spectra the spectral region of the atmospheric contributions has been removed and replaced by a straight line.

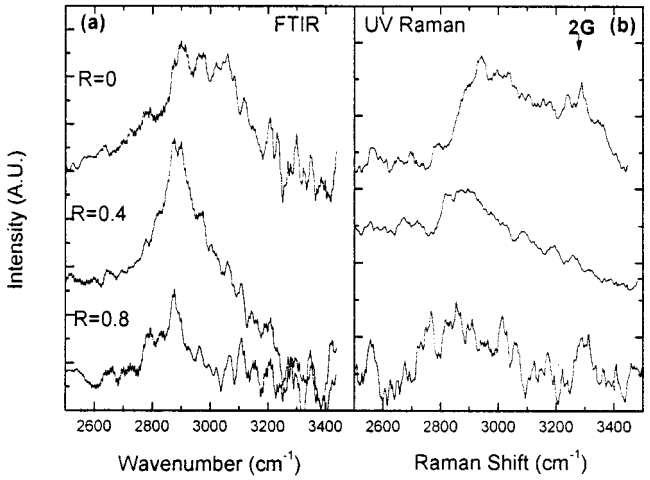

FIG. 11. Comparison of (a) FTIR spectra and (b) UV Raman spectra for a-C_{1-x}:Si_x:H_y alloys grown at $R=0$, 0.4, and 0.8 in the C–H_x stretching region. The spectra have been smoothed for clarity.

$R\sim0.6$, then increases towards ~3.2, typical of a-Si:H. The refractive index is similar to that of ta-C:H (Ref. 36) for $R<0.8$, $x<0.5$–0.6, and the main increase occurs in Si-rich alloys. The relationship between the refractive index and the Si/C ratio is not linear as reported by Jiang *et al.*,[43] so the refractive index is not such a good indicator of the film composition as was asserted there.

Figure 13 shows the optical gap (E_{04} and E_{Tauc}) as a function of R. E_{04} starts at ~2.25 eV, typical of ta-C:H, remains constant for R in the range from 0 to 0.3, and then rises to a maximum of ~3.25 eV for $R=0.7$–0.8, corresponding to $x\sim0.4$–0.6, before decreasing towards values typical of a-Si:H. This is a dependence found by many groups using PECVD.[47,74,75] The maximum at $R=0.7$–0.8 confirms that the stoichiometric composition $x=0.5$ occurs at this gas flow ratio.

The compositional dependence is consistent with the band model of Robertson.[75] The band gap is determined by different states in each composition range. In the C-rich alloys, the gap is determined by the π states of C sp^2 sites. The gap depends on the degree of clustering of sp^2 sites, or on the distortion of π bonds. Increasing the Si content from $x=0$ dilutes the amount of C–C bonds and reduces the cluster size, and this increases the band gap. In the Si-rich alloys, the band gap is determined by the Si–Si bond states. Increasing the C fraction replaces Si–Si bonds with Si–C bonds. These have a wider gap than the Si–Si bonds, so they lie away from the band edges. Thus the band gap increases with increasing C content from $x=1$ as the Si–Si bonds are diluted by Si–C bonds. The combination of these two effects causes a maximum in the band gap around $x=0.5$. The maximum lies close to $x=0.5$ when the hydrogen content is con-

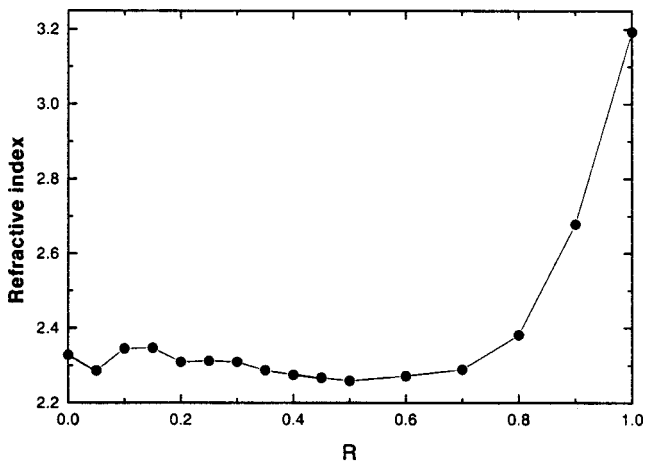

FIG. 12. Refractive index at 633 nm of a-C_{1-x}:Si_x:H_y alloys vs R.

Downloaded 04 Dec 2006 to 129.169.177.41. Redistribution subject to AIP license or copyright, see http://jap.aip.org/jap/copyright.jsp

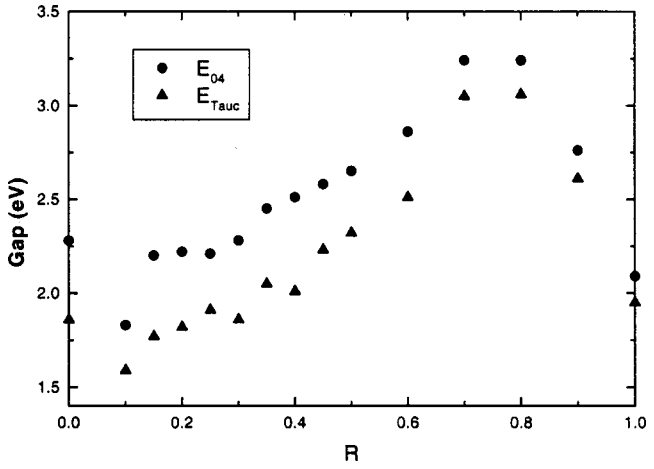

FIG. 13. Optical gap $a\text{-}C_{1-x}:Si_x:H_y$ alloys vs R.

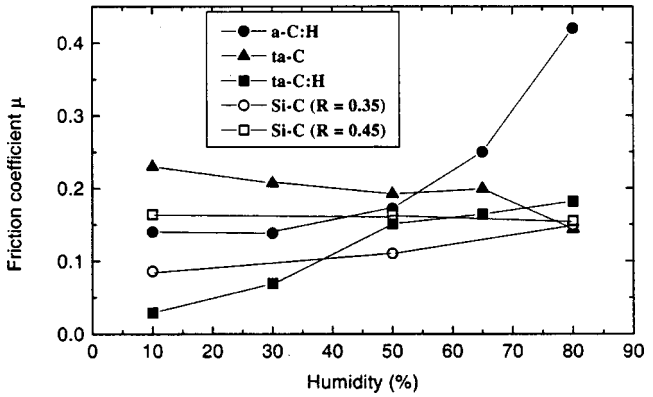

FIG. 15. Friction coefficient as a function of humidity for a a-C:H, ta-C:H, ta-C, and $a\text{-}C_{1-x}:Si_x:H_y$ alloys grown at $R=0.45$ and $R=0.35$ ($x=0.15-0.2$)

stant, as here, but it moves to C-rich compositions if the H content rises with C content as in PECVD films.[47,59,75]

G. Mechanical properties

A primary reason to study Si alloys is the reduction of stress. ta-C:H films have rather large stress compared to a-C:H because of the larger role of ions in the deposition. Figure 14 shows the stress as a function of R. A stress reduction of ~45% is observed for $R=10\%$, with a further fall after $R=0.6$ to an almost complete stress relief. The initial fall of 45% is similar to that reported by Gangopadhyay *et al.*[22] for films grown at a fixed bias voltage. The lower stress allows films thicker than 500 nm to be grown at $R=0.2$ and 0.4, compared to only about 100 nm for ta-C:H itself. This is a very useful improvement. Note that our ta-C:H deposited by ECWR has a much higher stress of ~6–7 GPa than the 1–2 GPa in PECVD diamond-like a-C:H, for which Si alloying was previously studied.[22,32]

The Young's modulus of as-deposited ta-C:H films measured by Brillouin scattering is ~300 GPa,[39] with a Poisson's ratio of about 0.3. A hardness of ta-C:H was previously derived as 55 GPa,[36] but this may be an overestimate. Nanoindentation was performed on thick (>500 nm) samples grown at $R=0.2$ and 0.4, and hardness values of at least 15 GPa were found. This is low compared to the original value for ta-C:H itself, and the cause of this is being checked further.

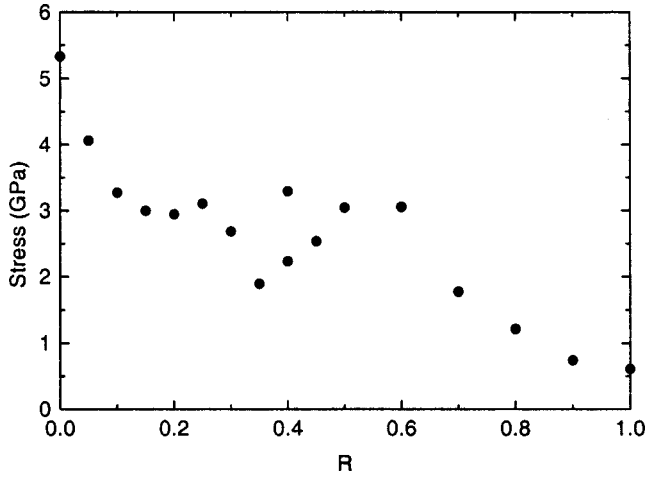

FIG. 14. Stress of $a\text{-}C_{1-x}:Si_x:H_y$ alloys vs R.

We deposited a series of standard ta-C and diamond-like a-C:H films by filtered cathodic vacuum arc and PECVD, respectively. These films were used to compare the friction behavior for the standard amorphous carbon systems ta-C, ta-C:H, and diamond-like a-C:H, together with the series of $a\text{-}C_{1-x}Si_x:H_y$. The friction measurements on all these samples were performed in the same conditions in the same friction rig. Friction measurements at different laboratories can show considerable variation, presumably because of the specific test conditions of load, velocity, surface conditions, etc. Our tests allow a comparison of a wide range of diamond-like carbon films under a particular set of conditions.

Figure 15 compares our steady friction coefficients of a-C:H, ta-C, and ta-C:H films measured with a steel ball. The friction coefficient (μ) of our a-C:H is seen to increase with increasing humidity, but it does not achieve the very low values of 0.05 at low humidity found by Enke *et al.*,[12] but it is consistent with other authors.[17,20,76] The friction coefficient of ta-C is seen to be higher than that of a-C:H at low humidity, but still quite low, 0.23. It then falls slightly with increasing humidity. This behavior is the same as that found for ta-C deposited by laser ablation by Voevodin *et al.*[33] We see that ta-C:H behaves midway between a-C:H and ta-C. Its friction coefficient is very low at low humidity, rises at higher humidity, but then saturates at about 0.15 at high humidity. Thus ta-C:H without Si already shows excellent friction properties in the range 10%–80% humidity ($\mu=0.06-0.12$).

Figure 16 shows the friction coefficients of $a\text{-}C_{1-x}Si_x:H_y$ alloys at three relative humidity values. The friction was measured against both steel and diamond-like a-C:H coated steel balls. We see that the presence of up to 20%–30% silicon ($R=0.6$) does not greatly affect the friction coefficient. This is true for both types of balls, which is consistent with previous results.[22] It seems therefore that Si addition stabilizes the friction coefficient at roughly

Downloaded 04 Dec 2006 to 129.169.177.41. Redistribution subject to AIP license or copyright, see http://jap.aip.org/jap/copyright.jsp

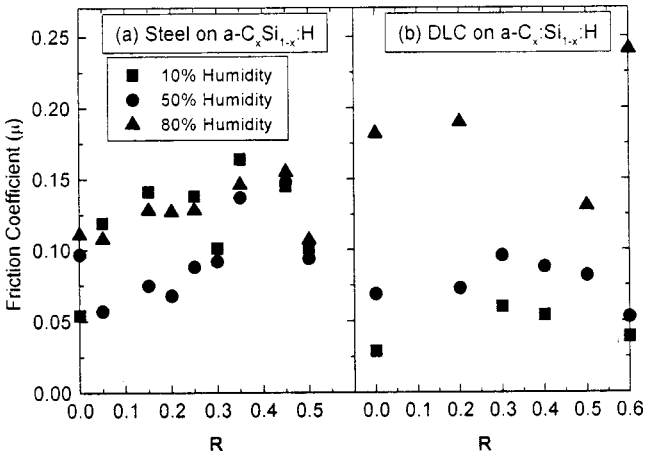

FIG. 16. Friction coefficient at 10%, 50%, and 80% humidity for a-C_{1-x}:Si_x:H_y alloys vs R for (a) steel ball and (b) diamond-like a-C:H coated steel ball.

0.1–0.15. This is less than for ta-C at room atmosphere, and is comparable to that obtained with Si in a-C:H.[16,19]

Film failure was observed with $\mu \sim 0.6$ for $R > 0.5$ with steel balls and $R > 0.6$ with an a-C:H coated ball, corresponding to films with less carbon. This behavior is similar to that found by other authors.[76,17] The higher friction coefficient may be due to a more SiC-like surface, which generally shows higher friction.[77] This is consistent with our finding that for $R > 0.6$ the homopolar C=C bonds tend to disappear as well as the lower density surface layer.

Figure 15 also compares the friction coefficient at different humidity for two a-$C_{1-x}Si_x$:H_y films with a Si content of under 0.2 with those of ta-C, a-C:H, and ta-C:H against a steel ball. The data show that the friction coefficient of a-$C_{1-x}Si_x$:H_y films with $x = 0.1$–0.2 are almost independent of humidity in the range studied. This is similar to that found previously for PECVD a-$C_{1-x}Si_x$:H_y alloys:[12–14] a low friction only for Si contents between 0.03 and 0.2.

The different friction behavior of ta-C, ta-C:H, a-C:H, and a-$C_{1-x}Si_x$:H_y films is understood as follows. In a-C:H films at low humidity, wear causes a hydrocarbon-rich microfilm to be transferred to the counterbody of the tribological system. The presence of C:H films on both surfaces now provides a low friction. However, at high humidity there is little film transfer to the counterbody, so the friction coefficient remains high.[33,78] In ta-C micro-Raman measurements show that wear creates a graphitic wear track and also transfers some graphitic carbon to the countersurface.[33] The graphitic surfaces have a relatively low friction, but not as low as C:H surfaces. A high humidity causes water to intercalate between the graphitic atomic layers and this lowers the friction coefficient. ta-C:H is seen to have good friction properties at all humidities. The good friction performance of ta-C:H at high humidity probably arises because its wear track and transfer layer are more graphitic, as in ta-C, as also indicated by our reflection EELS measurements.

In PECVD a-$C_{1-x}Si_x$:H_y wear creates a layer of hydrated silica which can act as a lubricant in a humid environment.[16,17] Therefore the residual siloxane (Si–O) bond plays an important role in the reduction of the friction coefficient of a-C:H in a high humidity atmosphere.[79] In ta-C:H, the addition of Si is not needed to retain a low friction coefficient in humid conditions. In this case, Si causes the friction coefficient to be essentially independent of humidity as seen in Figs. 15 and 16(a). Perhaps the hydrated silica mechanism is unable to operate in the case of ta-$C_{1-x}Si_x$:H_y, so the alloys do not have such low friction coefficients at low humidity.

Figure 16(b) shows the friction coefficient increasing with the humidity, when the steel ball is coated with a-C:H. This increase is due to the worsening of the friction properties of the a-C:H coated ball and does not depend on the a-$C_{1-x}Si_x$:H_y film.

IV. CONCLUSION

This work shows that the ECWR source can be used for the high rate deposition of a-$C_{1-x}Si_x$:H_y alloys, ranging from ta-C:H to a-Si:H. The structural, optical, and tribological properties of these alloys were analyzed. We show how UV Raman spectroscopy allows a direct detection of Si–C, Si–H, and C–H bonds, unlike visible Raman spectroscopy, and is complementary to infrared spectroscopy. The incorporation of Si causes the size of the C sp^2 clusters to decrease and opens C sp^2 rings. Si also reduces the internal compressive stress of the a-$C_{1-x}Si_x$:H_y films compared to ta-C:H. This allows us to deposit films thicker than 500 nm.

This work has shown how ta-C:H films have a low, almost humidity insensitive friction coefficient of ~ 0.05–0.15. A small Si introduction, $x \sim 0.1$, allows a $\sim 45\%$ reduction in the stress, while maintaining the low friction and low humidity sensitivity. Coatings with relatively high hardness, low stress, low and humidity insensitive friction, and an optical gap of 2.5 eV can be deposited, satisfying the requirements for a wide range of possible applications.

ACKNOWLEDGMENTS

The authors would like to thank D. Batchelder of Leeds University and D. Richards of Cavendish Laboratory, Cambridge, for Raman facilities, V. Paret for RBS and ERDA measurements, A. LiBassi and B. K. Tanner of Durham University for XRR measurements, R. A. P. Smith and N. L. Rupesinge for XPS data, S. E. Rodil and V. Stolojan for EELS measurements, S. Schreiber for help in the system design and construction, and UK EPSRC for financial support. A. C. F. acknowledges funding by an EU TMR Marie Curie fellowship.

[1] J. Bullot and M. P. Schmidt, Phys. Status Solidi B **143**, 345 (1985).
[2] Y. Tawada, K. Ysuge, M. Kondo, H. Okamaoto, and Y. Hamakawa, J. Appl. Phys. **53**, 5273 (1982).
[3] A. H. Mahan, D. L. Williamson, B. P. Nelson, and R. S. Crandall, Appl. Phys. Lett. **55**, 783 (1989).
[4] A. Matsuda and K. Tanaka, J. Non-Cryst. Solids **97**, 1367 (1987).
[5] W. A. Nevin, H. Yamagishi, M. Yamaguchi, and Y. Tawada, Nature (London) **368**, 529 (1994).
[6] T. Ma, J. Xu, J. Du, W. Li, X. Huang, and K. Chen, J. Appl. Phys. **88**, 6408 (2000).
[7] J. Robertson, Adv. Phys. **35**, 317 (1986).
[8] J. Robertson, Surf. Coat. Technol. **50**, 185 (1992).
[9] J. Robertson, Prog. Solid State Chem. **21**, 199 (1991).

Downloaded 04 Dec 2006 to 129.169.177.41. Redistribution subject to AIP license or copyright, see http://jap.aip.org/jap/copyright.jsp

[10] K. Enke, Thin Solid Films **217**, 56 (1981).
[11] M. A. Tamor, Mater. Res. Soc. Symp. Proc. **383**, 423 (1995).
[12] K. Enke, H. Dimigen, and K. Hübsch, Appl. Phys. Lett. **36**, 291 (1980).
[13] R. Memming, H. J. Tolle, and P. E. Wierenga, Thin Solid Films **143**, 31 (1986).
[14] B. Dischler, A. Bubenzer, and P. Koidl, Solid State Commun. **48**, 105 (1983).
[15] K. Oguri and T. Arai, J. Mater. Res. **5**, 2567 (1990).
[16] K. Oguri and T. Arai, Surf. Coat. Technol. **47**, 710 (1991).
[17] K. Oguri and T. Arai, J. Mater. Res. **7**, 1313 (1992).
[18] K. Oguri and T. Arai, Thin Solid Films **208**, 158 (1992).
[19] J. Meneve, E. Dekempeneer, R. Jacobs, L. Eersel, V. Van Den Bergh, and J. Smeets, Diamond Relat. Mater. **1**, 553 (1992).
[20] J. Meneve, E. Dekempeneer, and J. Smeets, Diamond Films Technol. **4**, 23 (1994).
[21] J. Meneve, E. Dekempeneer, W. Wegener, and J. Smeets, Surf. Coat. Technol. **86–87**, 617 (1996).
[22] A. K. Gangopadhyay, P. A. Willermet, M. A. Tamor, and W. C. Vassel, Tribol. Int. **30**, 9 (1997).
[23] S. S. Camargo, Jr., A. L. Baia Neto, R. A. Santos, F. L. Freire, Jr., R. Carius, and F. Finger, Diamond Relat. Mater. **7**, 1155 (1998).
[24] A. C. Ferrari, B. Racine, N. A. Morrison, I. Hutchings, W. I. Milne, and J. Robertson, Mater. Res. Soc. Symp. Proc. **593**, 523 (1999).
[25] J. Robertson, Diamond Relat. Mater. **3**, 361 (1994).
[26] D. R. McKenzie, D. Muller, and B. A. Pailthorpe, Phys. Rev. Lett. **67**, 773 (1991).
[27] T. A. Friedmann, K. F. McCarty, J. C. Barbour, M. P. Siegal, and D. C. Dibble, Appl. Phys. Lett. **68**, 1643 (1996).
[28] A. C. Ferrari, B. Kleinsorge, N. A. Morrison, A. Hart, V. Stolojan, and J. Robertson, J. Appl. Phys. **85**, 7191 (1999).
[29] X. Jiang, W. Beyer, and K. Reichelt, J. Appl. Phys. **68**, 1378 (1990).
[30] Z. L. Akkerman, H. Efstathiadis, and F. W. Smith, J. Appl. Phys. **80**, 3068 (1996).
[31] A. Erdemir, O. L. Eryilmaz, and G. Fenske, J. Vac. Sci. Technol. A **18**, 1987 (2000).
[32] C. Donnet, Surf. Coat. Technol. **100**, 180 (1998).
[33] A. A. Voevodin, A. W. Phelps, J. S. Zabinski, and M. S. Donley, Diamond Relat. Mater. **5**, 1264 (1996).
[34] X. Jiang, K. Reichelt, and B. Stritzker, J. Appl. Phys. **66**, 5805 (1990).
[35] M. Weiler, S. Sattel, K. Jung, H. Ehrhardt, and J. Robertson, Appl. Phys. Lett. **64**, 2797 (1994).
[36] M. Weiler, S. Sattel, T. Giessen, K. Jung, H. Ehrhardt, V. S. Veerasamy, and J. Robertson, Phys. Rev. B **53**, 1594 (1996).
[37] M. Weiler, K. Lang, E. Li, and J. Robertson, Appl. Phys. Lett. **72**, 1314 (1998).
[38] N. A. Morrison, S. Muhl, S. E. Rodil, A. C. Ferrari, M. Nesladek, W. I. Milne, and J. Robertson, Phys. Status Solidi A **172**, 79 (1999).
[39] A. C. Ferrari, J. Robertson, M. G. Beghi, C. E. Bottani, R. Ferulano, and R. Pastorelli, Appl. Phys. Lett. **75**, 1893 (1999).
[40] A. C. Ferrari, A. Libassi, B. K. Tanner, V. Stolojan, J. Yuan, L. M. Brown, S. E. Rodil, B. Kleinsorge, and J. Robertson, Phys. Rev. B **62**, 11089 (2000).
[41] X. Zhang, W. H. Weber, W. C. Vassell, T. J. Potter, and M. A. Tamor, J. Appl. Phys. **83**, 2820 (1998).
[42] W. K. Choi, Y. M. Chan, C. H. Ling, Y. Lee, R. Gopalakrishnan, and L. Tan, J. Appl. Phys. **77**, 827 (1995).
[43] L. Jiang, X. Chen, X. Wang, L. Xu, F. Stubhan, and K. Merkel, Thin Solid Films **352**, 97 (1999).
[44] F. DeMichelis, F. Giorgis, C. F. Pirri, and E. Tresso, Philos. Mag. B **71**, 1015 (1995).
[45] V. Chu, J. P. Conde, J. Jarego, P. Brogueira, J. Rodriguez, N. Barradas, and J. C. Soares, J. Appl. Phys. **78**, 3164 (1995).
[46] I. Solomon, M. P. Schmidt, and H. Tran-Quoc, Phys. Rev. B **38**, 9895 (1988).
[47] J. P. Conde, V. Chu, A. Kling, Z. Dai, J. C. Soares, S. Arekat, A. Fedorov, M. N. Berberan-Santos, F. Giorgis, and F. Pirri, J. Appl. Phys. **85**, 3327 (1999).
[48] S. F. Yoon and J. Ahn, J. Vac. Sci. Technol. A **15**, 1832 (1997).
[49] R. W. B. Pease and A. G. Gaydon, *Identification of Molecular Spectra* (Chapman and Hall, London, 1963).
[50] *CRC Handbook of Chemistry and Physics*, 80th ed., edited by D. Lide (CRC Boca Raton, FL, 1999), pp. 9-64 and 10-178.
[51] R. J. Kee, F. M. Rupley, and J. A. Miller, Sandia Report No. SAND87-8215B, 1990 (unpublished), p. 10.
[52] W. Beyer, J. Non-Cryst. Solids **97**, 1027 (1987).
[53] E. Gogolides, D. Mary, A. Rhallabi, and G. Turban, Jpn. J. Appl. Phys., Part 1 **34**, 261 (1995).
[54] J. Ristein, R. T. Stief, L. Ley, and W. Beyer, J. Appl. Phys. **84**, 3836 (1998).
[55] B. L. Henke, E. M. Gullikson, and J. C. Davis, At. Data Nucl. Data Tables **54**, 181 (1993).
[56] G. Lucovsky, R. J. Nemanich, and J. Knights, Phys. Rev. B **19**, 2064 (1979).
[57] H. Wieder, M. Cardona, and C. R. Guarnieri, Phys. Status Solidi B **92**, 99 (1979).
[58] S. Akita, K. Wakita, Y. Nakayama, and T. Kawamura, in *Amorphous and Crystalline Silicon Carbide*, edited by G. L. Harris and C. Y. W. Yang (Springer, New York, 1989), p. 77.
[59] M. Park, C. W. Teng, V. Sakhrani, M. B. Laurin, R. M. Kolbas, R. C. Sanwald, R. J. Nemanich, J. J. Hren, and J. J. Cuomo, J. Appl. Phys. **89**, 1130 (2001).
[60] G. Lucovsky, Solid State Commun. **29**, 571 (1977).
[61] N. M. J. Conway, A. C. Ferrari, A. J. Flewitt, J. Robertson, W. I. Milne, A. Tagliaferro, and W. Beyer, Diamond Relat. Mater. **9**, 765 (2000).
[62] A. C. Ferrari and J. Robertson, Phys. Rev. B **61**, 14095 (2000).
[63] S. Gorman and S. A. Solin, Solid State Commun. **15**, 761 (1974).
[64] M. Ramsteiner, J. Wagner, C. Wild, and P. Koidl, Solid State Commun. **67**, 15 (1988).
[65] J. R. Shi, X. Shi, Z. Sun, E. Liu, H. S. Yang, L. K. Cheat, and X. Z. Jin, J. Phys.: Condens. Matter **11**, 5111 (1999).
[66] K. W. K. Gilkes, H. S. Sands, D. N. Batchelder, J. Robertson, and W. I. Milne, Appl. Phys. Lett. **70**, 1980 (1997).
[67] V. I. Merkulov, J. S. Lannin, C. H. Munro, S. A. Asher, V. S. Veerasamy, and W. I. Milne, Phys. Rev. Lett. **78**, 4869 (1997).
[68] A. C. Ferrari and J. Robertson, Phys. Rev. B **64**, 075414 (2001).
[69] K. Karch, P. Pavone, W. Windl, O. Shutt, and D. Strauch, Phys. Rev. B **50**, 17054 (1994).
[70] Y. Inoue, S. Nakashima, A. Mitsuishi, S. Tabata, and S. Tsuboi, Solid State Commun. **48**, 1071 (1983).
[71] A. Morimoto, T. Kataoka, M. Kumeda, and T. Shimizu, Philos. Mag. B **50**, 517 (1984).
[72] J. P. Gerault, R. Morancho, and G. Constant, Philos. Mag. B **49**, 11 (1984).
[73] F. Demichelis, C. F. Pirri, and E. Tresso, J. Appl. Phys. **74**, 1327 (1992).
[74] R. S. Sussman and R. Ogden, Philos. Mag. B **44**, 137 (1981).
[75] J. Robertson, Philos. Mag. B **66**, 615 (1992).
[76] A. Gangopadhyay, Tribol. Lett. **5**, 25 (1998).
[77] K. Miyoshi and D. H. Buckley, ASLE Trans. **22**, 79 (1979).
[78] K. Miyoshi, Surf. Coat. Technol. **43/44**, 799 (1990).
[79] T. Hioki, Y. Itoh, A. Itoh, S. Hibi, and J. Kawamoto, Surf. Coat. Technol. **46**, 233 (1991).

Downloaded 04 Dec 2006 to 129.169.177.41. Redistribution subject to AIP license or copyright, see http://jap.aip.org/jap/copyright.jsp